Next-Generation OFDMA-Based Passive Optical Network Architecture Supporting Radio-Over-Fiber

Yu-Min Lin, *Member, IEEE,* and Po-Lung Tien, *Member, IEEE*

***Abstract*—In this paper, we propose a novel architecture for next-generation orthogonal frequency division multiple access (OFDMA)-based passive optical networks (PON's), referred to as ROFPON. Besides carrying local broadband OFDMA data, ROFPON seamlessly supports radio-over-fiber (RoF) transports between the central office and multiple remote antennas at end users without using costly WDM lasers. We analytically and experimentally study the receiver sensitivity to OFDMA signals and the radio frequency (RF) signal's performance. By corroborating simulation results with experimental results, we discuss the determination of crucial system parameters, such as the optimal broadband-to-radio power ratio, and the exploitation of a notch filter for removing RF interference. Experimental results show that the integrated 10 Gb/s OFDMA and three 20 MHz RF signals are successfully transported both downstream and upstream over a 20 km single-mode-fiber PON. Finally, experimental results demonstrate that QPSK-encoded WiMAX-format RF signals are transmitted/relayed upstream with E-O-E conversion at each optical network unit (ONU), and received error-free at the optical line terminal after cascading 32 ONU's.**

***Index Terms*—orthogonal frequency division multiplexing access (OFDMA), passive optical network (PON), radio over fiber (RoF), radio frequency (RF), optical fiber communication, optical modulation.**

I. Introduction

ACCOMPANYING the growing trend to deploy optical fibers deeper into subscriber premises, is an increased entry of passive optical networks (PON's) into the wireline access market to provide higher data rates for future bandwidth-hungry real-time applications. Today, the gigabit passive optical network (GPON) offers downstream and upstream bit rates of 2.5 Gbit/s and 1.25 Gbit/s, respectively. This solution is based on the non-return-to-zero (NRZ) modulation format, where more than 32 subscribers share the bandwidth by time division multiplexing (TDM) [1]. However, with the rapid growth of high-speed services like Internet protocol television (IPTV) and high-definition (HD) video, a further increase in bandwidth over 10 Gb/s in access networks is needed. Directly using a 10 Gb/s line rate system is indeed a viable solution [2], but such a system's components may be prohibitively expensive. Wavelength division multiplexing (WDM) PON's [3] provide dedicated channels to each user by adopting costly WDM lasers and multiplexers. Therefore, to increase the bandwidth up to 10 Gbit/s while keeping costs acceptable, recent work has turned to orthogonal frequency division multiplexing (OFDM), envisioning this as a promising modulation format for next generation PON's [4,5,6,7,8]. Furthermore, with quadrature amplitude modulation (QAM) used for the subcarriers of OFDM symbols, the bandwidth requirement of optical and electrical components can be reduced. Additionally, the inherent frequency diversity of OFDM transmission enables simple equalization of frequency response by means of baseband digital signal processing. This feature can be used not only to mitigate the fiber's dispersion [9], but also to solve the frequency ripple problem caused by the use of low cost components.

In parallel with the evolution of PON's, there is an increasing demand of wireless access for greater bandwidth and longer reach. One of the approaches is to miniaturize the cell size to increase network capacity. However, it gives rise to a high-cost backhauling deployment hurdle. To this end, recent work has focused on integrating radio signals over high capacity fibers, referred to as radio-over-fiber (RoF) [10,11,12]. With the increasingly deep penetration of PON infrastructure into users' premises, RoF can be realized by placing low-power small-size remote antenna ports at the optical network units (ONU's) of the PON's. Such a design eliminates the need of allocating base stations for longer reach, thereby greatly reducing the hardware complexity. Accordingly, this integration takes advantage of the high capacity of the optical fiber while reducing deployment cost.

Much work has explored the possibility of integrating RoF into the PON environment. The WDM PON in [13] uses a dedicated wavelength to support each radio frequency (RF) channel to transport a narrow band radio signal for each remote antenna. Such a design results in high cost and a scalability problem. Specifically, to support multiple RF channels, the approach expensively requires multiple optical receivers at the optical line terminal (OLT) of the PON's. Furthermore, the total number of wavelengths increases with the number of wireless systems' cells, rendering the system not scalable. For supporting single remote antenna, other approaches [14,15] use high-frequency subcarrier to transport the RF signal while PON data remains in the baseband. These methods successfully integrate both signals at the cost of high frequency components because the guard band between baseband and RF signals raises the bandwidth requirement. In a similar line of work, the carrier suppression-based RoF system [16] provides high-frequency RF-signal generation capabilities through using a complex Mach-Zehnder modulator.

For supporting multiple remote antenna ports over one trunk fiber, the use of one single optical receiver at the OLT to detect multiple wavelength channels results in the optical

Manuscript received 30 August 2009; revised 20 January 2010. This work was supported by the NCTU/ICL Joint Research Center, Taiwan, under Contract 9352BA4112.

Y. Lin is with the Information and Communications Research Labs, Industrial Technology Research Institute, Taiwan (e-mail: ymlin5@yahoo.com).

P. Tien is with the Department of Electrical Engineering, National Chiao Tung University, Taiwan (e-mail: polungtien@gmail.com).

Digital Object Identifier 10.1109/JSAC.2010.100804.

beat interference (OBI) problem [17]. OBI occurs when the frequencies of two or more laser sources are too close such that the frequency of undesired product terms (after the square-law photo detection) falls into the same bandwidth where signals reside, thereby causing interference. To alleviate this problem, the work proposed in [18] exploits frequency division multiplexing (FDM) on RF signals, and multiple upstream lasers at specially selected wavelengths (spaced widely apart from each other) for broadband PON data, to prevent electrical interference and OBI, respectively. On the whole, the problem remains challenging and unresolved. The main goal of our work is to tackle the problem from an architectural perspective.

In this paper, we propose a novel architecture for next-generation orthogonal frequency division multiple access (OFDMA)-based PON's, referred to as ROFPON [7,8]. ROFPON seamlessly integrates RoF signals with the local broadband data without using costly WDM lasers. It supports multiple remote antenna ports at ONU's with the use of only one optical receiver at the OLT while completely eliminating the OBI problem. Via experimentation and analysis, we study the receiver sensitivity to OFDMA signals and the RF signal's performance. By corroborating simulation results with experimental results, we discuss the determination of crucial system parameters, such as the optimal broadband-to-radio power ratio, and the exploitation of a notch filter for removing RF interference. Experimental results show that ROFPON allows three 20 MHz wireless RF channels at the 2.1 GHz band (from three remote antenna ports) to be overlaid with a 10 Gb/s OFDMA-PON signal via a single wavelength. The integrated signals are successfully transported both downstream and upstream over a 20 km single-mode-fiber PON. Finally, experimental results demonstrate that QPSK-encoded WiMAX-format RF signals are transmitted/relayed upstream with E-O-E conversion at each ONU, and received error-free at the OLT after cascading 32 ONU's.

The remainder of this paper is organized as follows. In Section 2, we present the ROFPON architecture and elaborate on how broadband and wireless RF signals are integrated. In Section 3, we delineate the performance for OFDM signal over fiber via analytic and simulation results. In Section 4, we study the interference between OFDM and RF signals in ROFPON. Experimental set-up and results are shown in Section 5. Finally, conclusion remarks are given in Section 6.

II. ROFPON- Architecture and Signal Integration

ROFPON (see Figure 1) connects multiple ONU's to OLT through a passive optical distribution node (ODD), which is connected to the OLT via a long trunk fiber. Each ONU has one short section of feeder fiber to the ODD. ROFPON uses two wavelength channels, λ_d and λ_u, to convey downstream and upstream data, respectively. Channels are further divided into synchronous time slots, called frames. As shown in Figure 1, within each optical frame, downstream wireless signal is overlaid with the OFDM signals by occupying a separate frequency range. For signals passing downstream, the splitter in ODD generates multiple signal copies from the OLT and broadcasts the signal to each ONU through a splitter, a circulator, and a feeder fiber. Within each ONU,

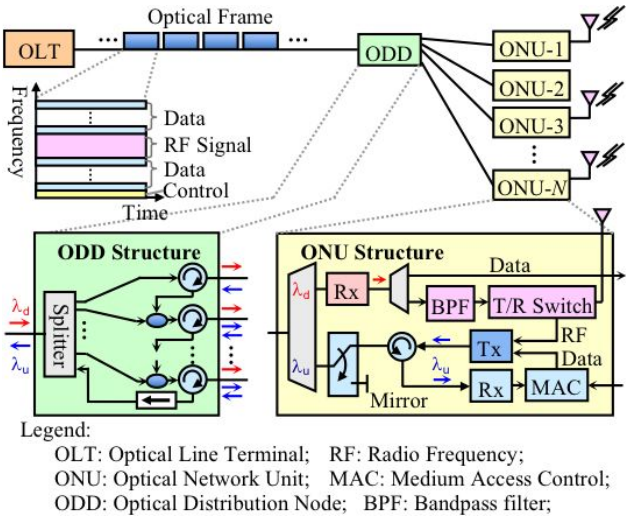

Fig. 1. ROFPON architecture.

after λ_d and λ_u are separated by a coarse WDM (CWDM), the downstream wavelength (λ_d) is received by the optical receiver, which converts the optical signal into the electrical form. Next, an electrical splitter separates the signal into two paths. Downstream OFDM data is demodulated in the first path, while in the second path, the wireless signal is filtered by a bandpass filter for wireless downlink communication.

For signals passing upstream on wavelength λ_u, ONU-1 first sends its upstream data and control information to ONU-2 through ODD's circulators and coupler. Notice that due to the use of OFDMA-based modulation, control information can be placed in pre-allocated subcarriers. Once the data/control is received by the upstream receiver module at ONU-2, its upstream medium access controller (MAC) performs bandwidth allocation to determine the subcarrier(s) for carrying the local upstream data. The MAC then regenerates the combined OFDMA signal by the upstream transmitter module and sends it to the next node, ONU-3. By the same token, the upstream signal is relayed point-to-point with an electrical-optical-electrical (E-O-E) conversion mechanism from ONU-3 until ONU-N. Note that dynamic bandwidth allocation must be used to govern the fair sharing of upstream bandwidth among all ONU's. Finally, at ONU-N, the upstream wavelength is passed to the OLT through the ODD and fiber. It is worth noting that, to prevent signal loss in the event of an accidental blackout or a shutdown of any ONU's, each ONU is additionally equipped with a protection switch for the upstream signal. If an ONU is inactive, its optical switch (see Figure 1) is set to being an optical mirror (i.e., the default state), reflecting incoming upstream wavelengths from the previous ONU back to the ODD.

Recall that the ROFPON system has been designed to accommodate multiple wireless signals received from different distributed antennas [19] located at different ONU's. Figure 2 illustrates how the multiple wireless RF signals are integrated and overlaid with the broadband OFDMA signals. In this example, two RF signals are received by two remote antennas (located at ONU-1 and ONU-2), respectively. In Figure 2, we show the spectra of both OFDM data and RF signal at

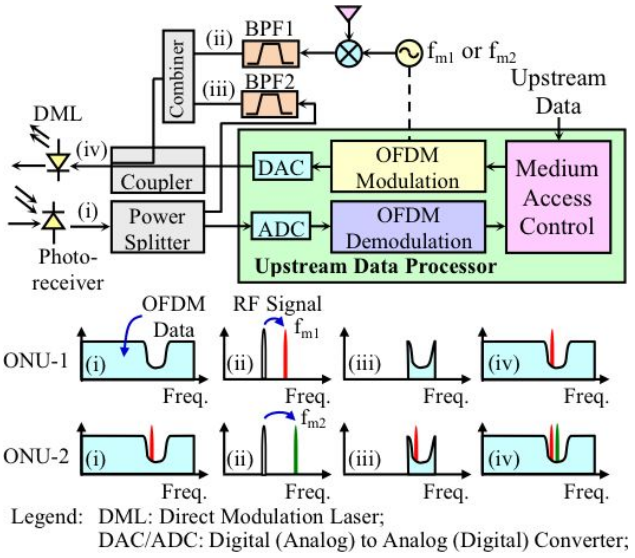

Fig. 2. Integration of OFDMA PON data and wireless RF signals.

four stages, (i) through (iv), at ONU-1 and ONU-2. First, as shown at ONU-1's stage (ii), the wireless signal received by an antenna is frequency-shifted to the allocated band by a mixer, an oscillator, and a bandpass filter (BPF) called BPF1. Note that we intentionally keep the band clear by inserting zeros on corresponding IFFT points. The shifted signal is then combined with the upstream OFDMA signal (see ONU-1's stage (iv)), which is sent together by the directed modulated laser to ONU-2. Note that because there are no subcarriers in the allocated band, interference between the wireless signal and upstream OFDMA signal is controllable.

After having received the upstream wavelength from ONU-1, ONU-2 first splits the received signal into two paths. In the first path, the upstream OFDMA PON signal is regenerated by the upstream data processor. The entire process involves an analog to digital conversion, original OFDMA demodulation, control-channel identification, the addition of local data, the modulation of OFDMA signal regeneration, and finally, a digital to analog conversion. For the second path, the system uses a bandpass filter BPF2 on the allocated radio band to remove the OFDMA signal, while preserving all previous wireless signals, as shown in ONU-2's stage (iii). The RF combiner then combines the local antenna's signal from BPF1 with the previous ONU's wireless signals from BPF2. Finally, the system integrates the radio signal with the upstream OFDMA PON signal (see ONU-2's stage (iv)) via an RF directional coupler before driving the upstream laser. With this mechanism, multiple remote antennas' signals can be carried from ONU-1 to ONU-*N* and finally back to the OLT.

The proposed architecture has two main advantages. With the ring-based signal flow for upstream traffic, ROFPON eliminates the use of expensive upstream WDM lasers, and is free from the aforementioned OBI problem. It is worth noting that such advantages are achieved at the expense of two minor drawbacks. First, such a ring-based signal flow inherently induces additional propagation and OEO processing delays for upstream traffic. The propagation delay through many drop fibers (between ONU's) in the distribution cable

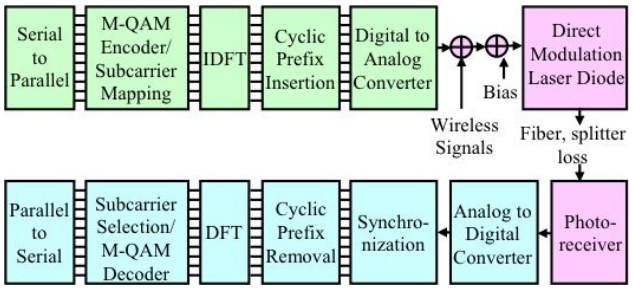

Fig. 3. OFDM over the IM-DD system.

section is only limited to several tens of microseconds. On the processing part, since there is no buffering delay, the OEO processing delay takes less than a microsecond under the 10-Gb/s line rate. Therefore, such fixed and short delay as a whole is irrelevant to the support of real time applications. The second drawback is the extra cost and insertion loss due to using more passive components in the ODD. Despite the fact that the ODD contributes several decibels of insertion loss between adjacent ONU's, in the following sections, we will demonstrate that the performance of upstream transport can accommodate such a power loss.

III. Performance of OFDM Signal over Fiber

Via analysis and simulations, in this section we study the bit-error-rate (BER) performance of OFDM signal over fiber under an intensity modulation-direct detection (IM-DD) system [20]. As shown in Figure 3, at the transmission end, broadband data is modulated with OFDM technology and converted to the optical domain by intensity modulation. (Note that intensity modulation can be performed using either a direct modulated laser or an external modulator integrated transmitter.) Specifically, the transmitter converts the incoming serial data into parallel M-QAM symbols. A subcarrier mapping is then used to distribute the symbols to the subcarrier locations for an N-point inverse discrete Fourier transform (IDFT). Note that in order to directly generate real-value waveforms for intensity modulation, symbols on the negative frequency points of IDFT are complex conjugates of the positive counterparts. Additionally, in the proposed OFDMA PON system, we intentionally skip several frequency points during the subcarrier mapping so that a relatively clear band is created for the RF signal. With IDFT, the symbols on the frequency domain are converted to time-domain waveform samples. The cyclic prefix is inserted to protect the inter-symbol-interference from the transmission link. Finally, the bias current is combined with the analog waveform from the digital to analog converter (DAC) to drive the optical transmitter.

At the receiving end, we adopt a cost effective form of direct detection that requires only one photodiode to reduce the complexity. Basically, the analog-to-digital converter (ADC) converts the waveform from the optical receiver to digital samples, in preparation for demodulation. The synchronizer is also used to extract the OFDM symbol boundary. After cyclic prefix (CP) is removed and the time-domain samples are converted to frequency-domain samples by DFT, the

demodulator makes the final decisions on the data subcarrier samples.

We now analyze the performance of OFDM signal with respect to the received OFDM signal power, P_{rec}. Given X_n that denotes the complex number representing a particular QAM constellation point carried on the n_{th} subcarrier, P_{rec} can be expressed as

$$P_{rec} = P_{in}\left[1 + m\mathrm{Re}\left\{\sum_{n=1}^{N_s} X_n \exp\left(j2\pi f_n t\right)\right\}\right], \quad (1)$$

where P_{in} is the received average optical power, N_S is the number of subcarriers, m is the modulation depth per subcarrier, and f_n is the n_{th} subcarrier's frequency. OFDM modulation is essentially a summation of single subcarrier multiplexing, except that they can be partially overlaid in frequency. Due to orthogonal properties during DSP de/modulation, every subcarrier's performance can be calculated separately. Thus, the average signal power (S) of a single subcarrier can be given by

$$S = \left(P_{in} \cdot m \cdot R\right)^2 / 2, \quad (2)$$

where R is the responsivity of a photodiode. In an unamplified system like PON, the receiver noise is the greatest obstacle to system performance. The receiver noise includes both thermal and shot noise. The total powers of the thermal and shot noise are given by $\sigma_{th}^2 = \frac{4KT}{R_e} \cdot F_e \cdot B$ and $\sigma_{sh}^2 = 2q \cdot R \cdot P_{in} \cdot B$, respectively, where K is the Boltzmann's constant, T is the absolute temperature, R_e is the load resistance, F_e is the receiver noise figure, B is the receiver bandwidth, and q is the electron charge. Note that in the OFDM signal, each subcarrier occupies twice the space as the subcarrier spacing, i.e., $B = 2\triangle f = 2 \cdot F_s/N$, where F_s and N represent the sampling rate and the fast Fourier transform (FFT) size of the OFDM DSP processor, respectively. (In the analytic computation and simulations, we adopt the following values: Responsivity $R = 0.9$, load resistance $R_e = 50$ Ohm, receiver noise figure $F_e =$ 2 dB, and $T = 300\,^{\circ}$K.) Given the signal and noise powers, the signal-to-noise ratio for the OFDM signal, SNR_{ofdm}, can be expressed as

$$SNR_{ofdm} = \frac{S}{\frac{4KT}{R_e} \cdot F_e \cdot B + 2q \cdot R \cdot P_{in} \cdot B}. \quad (3)$$

If the receiver's white noise is the main source of signal degradation, the BER of the Gray-coded M-QAM can be derived from the SNR and given by [26]

$$BER = \frac{2\left(1 - \frac{1}{\sqrt{M}}\right) erfc\left(\sqrt{\frac{3SNR}{2(M-1)}}\right)}{\log_2(M)}. \quad (4)$$

In addition to analytic results, we also use simulation results to demonstrate the BER performance of the OFDM signal. The individual subcarrier's performance can be measured from the error vector magnitude (EVM) of the receiver constellation as

$$EVM = \frac{\sqrt{\sum_{i=1}^{N_d} \frac{|D_i - r_i|^2}{N_d}}}{|D_{avg}|}, \quad (5)$$

where N_d is the total number of transmitted symbols per subcarrier, D_i and r_i are transmitted and received symbols, respectively, and D_{avg} represents the average amplitude of symbol points in the constellation diagram. With the EVM, one can estimate [21] the BER of each subchannel.

In the simulation, a total of 1 M data bits are generated and transmitted. At the receiver, the system BER is obtained by averaging the BER of all subchannels. The parameters for both analytical computation and simulation are given as follows. The ADC/DAC's sampling rate is 12 GHz, the FFT size is 2048, and the CP overhead is 1.56%. Random data is encoded in a 16-QAM format and placed in the subcarriers indexed from 8 to 485. The resulting signal occupies the spectral range from 46 MHz to 2841 MHz. To reserve the frequency band for a wireless signal, we skip 21 subcarriers during the subcarrier assignments to create a 123 MHz clear spectrum centered at 2130 MHz. Therefore, the total data subcarrier number is 457, and the total bit rate of the OFDM signal is 10.71 Gb/s (=12 G/2048 (subchannel symbol rate) $\times$ 457 (subcarriers) $\times$ 4 (bits/symbol in 16-QAM)). After considering 7% FEC [22] and 1.56% CP as overhead, the effective data throughput becomes 10 Gb/s.

Because the OFDM signal has an inherent high peak-to-average power ratio (PAPR), one needs a careful modulation index design when the signal is modulated on the laser diode. Under deep modulation index, the signal can occasionally be lower than the laser threshold and become clipped. On the other hand, reducing the driving power prevents clipping but causes the system to suffer from poor power efficiency, which is a crucial system performance index in an un-amplified optical link. We define the effective modulation index (μ) to be $\mu = m\sqrt{N_s}$, where m is the peak modulation depth of one subcarrier, and N_s is the number of data subcarriers. In Figure 4(a), we plot the back-to-back receiver sensitivity subject to achieving a BER of 10^{-9} under different μ values. The figure clearly shows that the optimum performance is achieved when μ is between 28% and 36%. Note that this result is only applied to the case with only broadband OFDM signal. When wireless signals are integrated with the OFDM signal, the modulation index of OFDM needs to be backed off to prevent the clipping problem described above. In Figure 4(b), we display both analytic and simulation results of the BER performance of the OFDM signal as a function of received optical power, under two μ values, 28.77% and 22.88% (2 dB back off). The figure shows that the simulation results are in agreement with analytic results. The figure serves as a guideline for the setting of the required optical power for OFDM signal. For example, since the state-of-the-art forward-error-correction (FEC) limit is 2×10^{-3}, to have an operational margin, we choose BER=10^{-4} as a performance criterion. We observe that the required optical power to achieve a BER=10^{-4} for OFDM signal with μ=22.88% is -15 dBm. This power value will be used in the experiment described later.

IV. Interference between OFDM-PON and RF Signals

For the integrated-signal system, the performance profoundly hinges on a crucial parameter- signal power ratio. In the following, we first give the definition, which is followed by the discussion on the interference. Recall that the RF signal is superimposed on the broadband OFDM signal, thereby

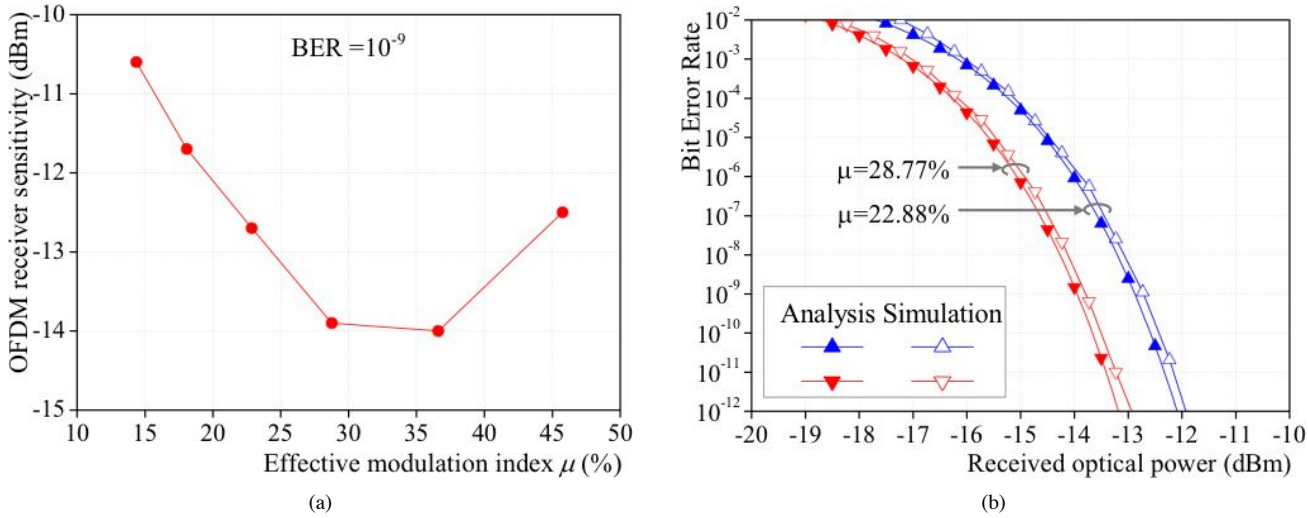

(a) (b)

Fig. 4. Performance of OFDM signals under the IM-DD system. (a) Receiver sensitivity under different μ's; (b) BER for the OFDM system.

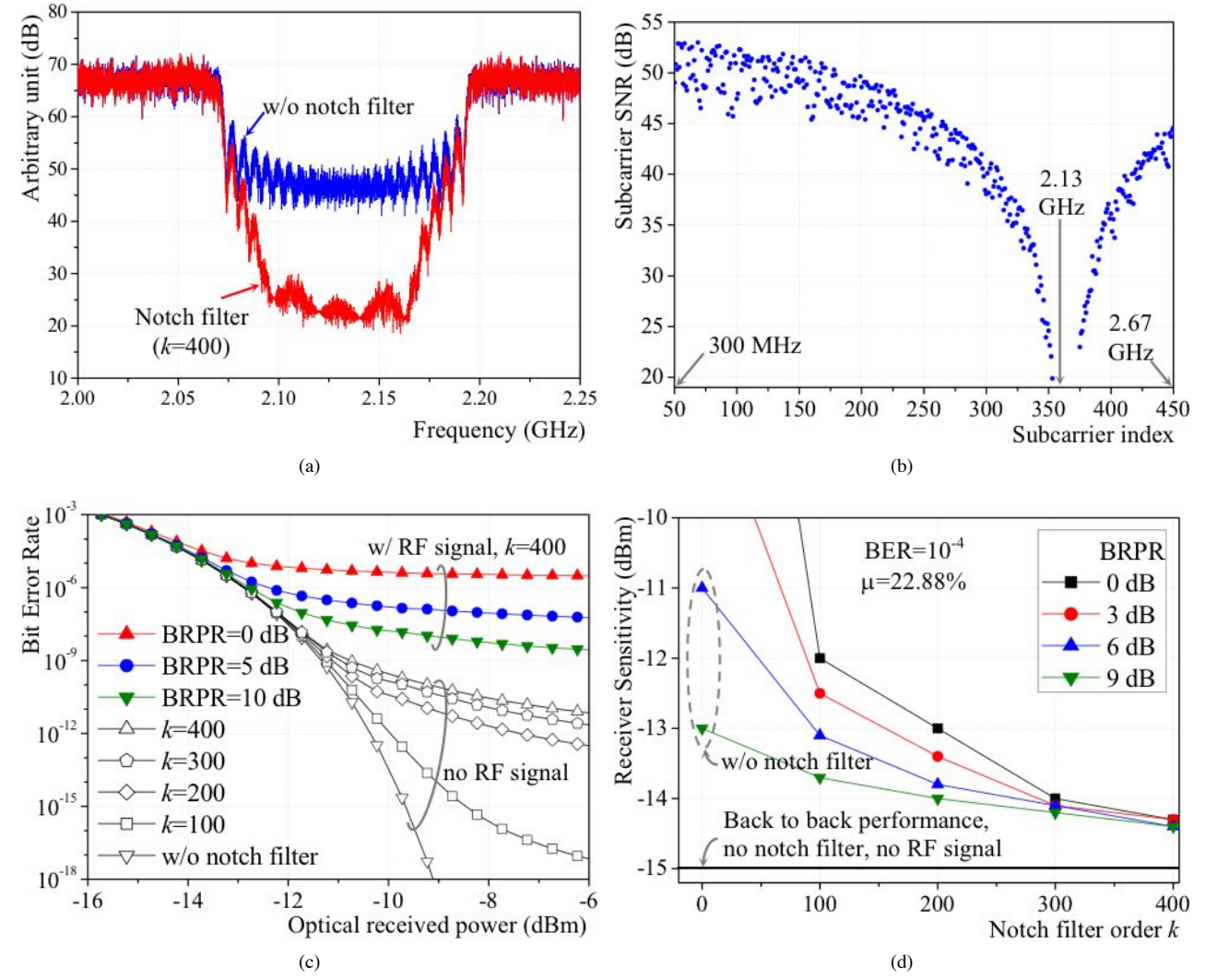

(a) (b)

(c) (d)

Fig. 5. Notch filters impact on OFDM signal performance. (a) Suppressed subcarriers side-lobes by notch filter; (b) Subcarriers SNR under k=400 notch filter; (c) OFDM BER under different filter orders; (d) Receiver sensitivity of OFDM signal.

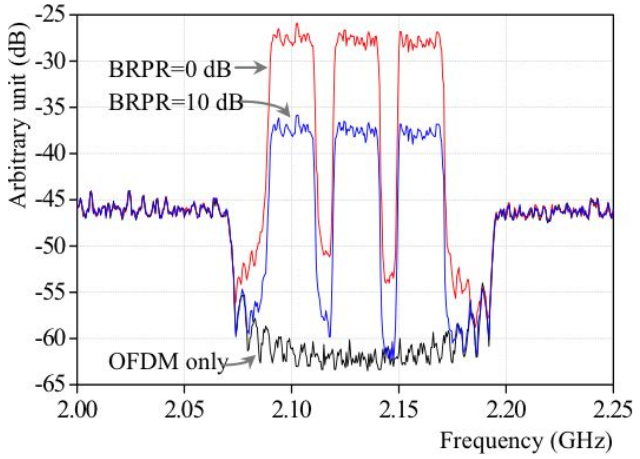

Fig. 6. Spectrum illustration on PON to RF interference.

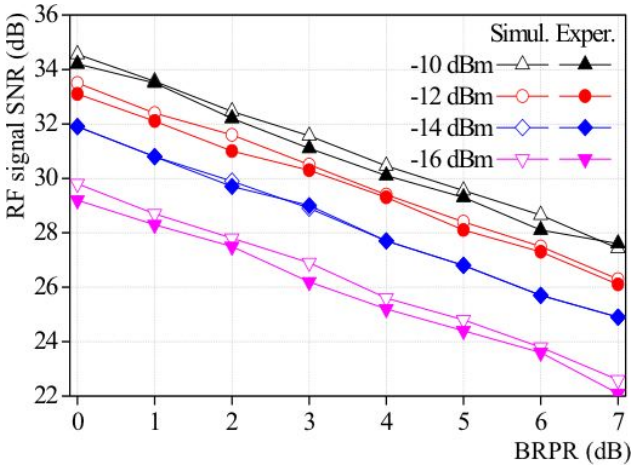

Fig. 7. RF signals SNR under different received powers.

yielding the driving power distribution to affect both signals. We define *broadband-to-radio power ratio (BRPR)* as

$$BRPR = \frac{\text{AveragePower}(OFDM)}{\text{AveragePower}(RF)}. \quad (6)$$

In the experiment on the integrated-signal system, three 20 MHz RF signals following the WiMAX physical format [23] are added to the OFDM signal before the laser diode is biased (see Figure 3). Because the WiMAX subcarriers are encoded in QPSK, the bit rate of each RF channel is 40 Mbps.

A. RF Signal Interference to OFDM-PON Signal

After the combined signal is received by the optical receiver, the OFDM receiver needs a notch filter after the ADC to remove the RF signal. However, introducing the notch filter at the radio band itself affects the orthogonality of nearby OFDM subcarriers. This phenomenon and impact is illustrated in Figure 5. In Figure 5(a) we show that the neighbor subcarriers' side-lobes are suppressed by the notch filter and that these subcarriers have already lost orthogonality to other subcarriers. To study the notch filter effect, we assess the OFDM signal performance by applying different filter orders, denoted as k. Note that the Keiser window method [24] is used to design the filter, while the filter's 100 MHz stopband depth is determined by the filter order. Figure 5(b) shows the subchannels' SNR after the filter of $k = 400$ is applied under an ideal electrical back to back case. It is clear that the subchannels around the radio band encounter significant penalty. Figure 5(c) shows the simulation results of the overall BER performance of the OFDM signal with different notch filter orders applied. From these results, we observe that using deeper notch filters results in higher error floors. However, a shallow notch filter cannot completely remove the RF signal.

There is also a trade-off between using different BRPR values and notch filter orders. Figure 5(d) shows the receiver sensitivity of the OFDM signal at BER=10^{-4} for different BRPR values, as a function of the notch filter order. When the RF signal is relatively weak, i.e. BRPR=9 dB, there is only a 1.5 dB difference of sensitivity between a $k = 100$ and a $k = 400$. However, when the RF signal is strong, we need a deeper notch filter to remove the interference from the RF signal. In the unique case that BRPR=0 dB, a notch filter with 400 taps can control the penalty within 0.7 dB (-15 dBm to -14.3 dBm), albeit at the cost of hardware complexity. Note that we also need to consider having a proper BRPR value to control the interference from the OFDM to the RF signal. Therefore, the selection of filter order also depends on the RF signals requirements. We then add the RF signal into the system with $k = 400$, under three BRPR values, and observe the OFDM signal performance. The simulation results are shown in Figure 5(c). The figure shows that when BRPR is 10 dB, the BER curves are dominated by the notch filter. When BRPR=0 dB, the error floor is lifted slightly, but the negligible power penalty is also observed (with BER=10^{-4}).

B. OFDM-PON Signal Interference to RF Signal

The existing of side lobes of neighboring OFDM subcarriers will interfere with the RF signal. The simulation results are shown in Figure 6. We present in the figure the RF spectrum under different BRPR values. It is clear that the BRPR value directly affects the signal to interference ratio (SIR) of RF signal. We also carried out a simulation to predict the performance of the RF signal in a point to point optical link. As shown in Figure 7, the results show that the recovered signal's SNR depends almost linearly on the BRPR value. When BRPR is increased from 0 dB to 6 dB, the wireless signal's SNR decreases from 34.5 dB to 28.5 dB at -10 dBm receiver power. In this case, the OFDM signal interference is a major factor in RF signal's performance.

C. Cascading Effect on the Upstream RF Signal

Recall that ROFPON adopts E-O-E conversion for relaying the upstream RF signal from ONU-1 to ONU-*N*, and from ONU-*N* to OLT through the splitter and trunk fiber. Therefore, the upstream link of a RF signal can be modeled as a chain of hops, as shown in Figure 8(a). Because the RF signal is re-transmitted without demodulation at each hop, as the signal propagates, the interference from the OFDM signal causes noise to accumulate along the ONU's. At each ONU, the RF signal passes through a coupler, an E-O-E conversion, and a BPF. The coupler combines the OFDM signal with the RF

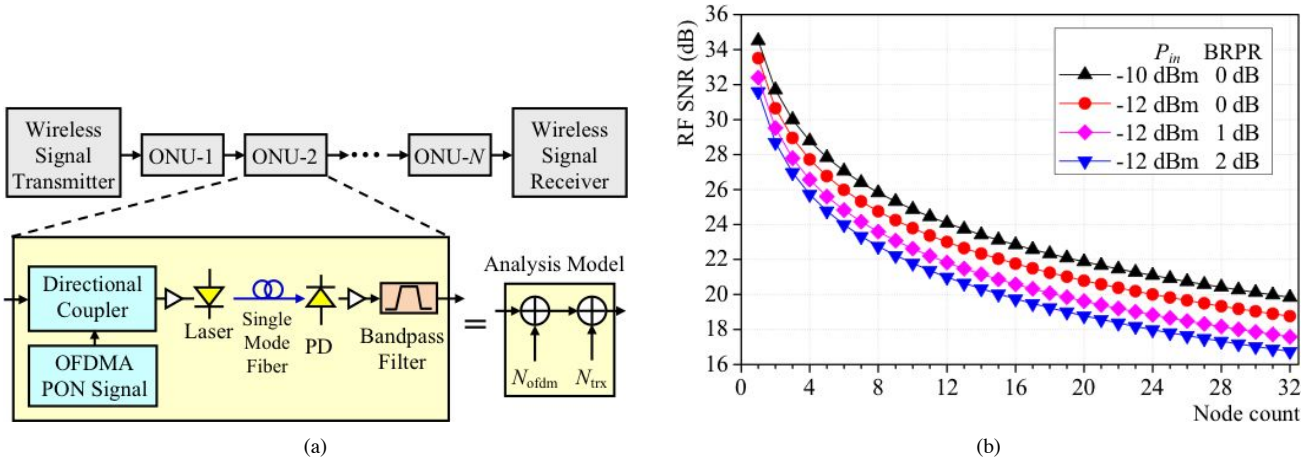

(a) (b)

Fig. 8. RF signal performance with respect to the number of cascading ONUs. (a) RF signal E-O-E relaying illustration; (b) Simulation result for the system model in (a).

signal and introduces interference, as described in the previous subsection. The BPF eliminates the OFDM signal outside the radio band, so it imposes no significant penalty to the RF signal. Therefore, as shown in Figure 8(a), we can re-model the blocks in one ONU as two noise sources, which are essentially the interference from the OFDM signal (N_{ofdm}), and noise originating from the E-O-E conversion process (N_{trx}). Note that in every ONU, besides being multiplexed with the local upstream OFDM-PON data, the upstream OFDM signal is also regenerated, so that the OFDM signal becomes uncorrelated with other ONU's OFDM signals. Provided that the OFDM signal's interference is also uncorrelated with the RF signal, we can actually treat the OFDM's interference as white noise and combine it with the N_{trx}, the optical transceiver induced noise, to predict the RF signal's performance after cascading ONU's. Assuming that the back-to-back wireless electrical transceiver is $SNR_0 = S/N_0$. If only ONU-1 is presented, the received signal's SNR_1 can be expressed as

$$SNR_1 = \frac{S}{N_0 + N_1}, \tag{7}$$

where S is the received signal power and $N_1 = N_{ofdm1} + N_{trx1}$ is the noise from ONU-1. In this architecture, we assume the received optical power and BRPR are kept the same for all ONUs, yielding $N_1 = N_2 = \cdots = N_u$. Hence, after the wireless signal travels through u ONU's, it's performance becomes

$$SNR_u = \frac{S}{N_0 + u \cdot N_1}. \tag{8}$$

By substituting N_1 with SNR_0 and SNR_1, SNR_u is given by

$$SNR_u = \frac{S}{N_0} \cdot \left(1 + u \cdot \left(\frac{SNR_0 - SNR_1}{SNR_1}\right)\right)^{-1}. \tag{9}$$

With Equation (9), we can now apply the SNR_1 result from Figure 7 to predict SNR performance after cascading ONU's. Simulation results are shown in Figure 8(b). Note that because the transceiver back to back SNR_0 is usually very high, we can assume $SNR_0 = 45$ dB (according to the experimental results). If the BRPR value is smaller than 2 dB and the optical received power is greater than -12 dBm, the wireless signal after 32 ONU's can maintain an SNR of 16 dB, which is the BER=10^{-9} boundary for a QPSK encoded wireless signal.

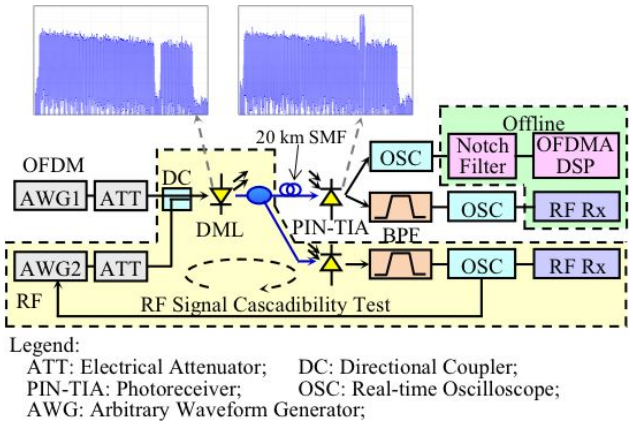

Fig. 9. Experimental setup.

V. Experimental Results and Discussions

A. Experimental Setup

We carried out an experiment to test the performance and viability of the ROFPON architecture. The experimental setup is illustrated in Figure 9. The experiment is divided into two parts. First, we evaluate the performance of both the OFDM and wireless RF signals when they are combined and transported over a 20 km optical link. The second part of the experiment assesses how the upstream RF signal is affected by the accumulated interference from the OFDMA signal. The OFDM signal, which occupies $0.05 \sim 2.8$ GHz of bandwidth, is generated offline with a DSP program. The IFFT size is 2048, from which 457 16-QAM encoded subcarriers are used for data transmissions. The raw data rate is 10.7 Gb/s, which includes 7% FEC overhead, yielding a network throughput of 10 Gb/s. To accommodate multiple RF signals, the allocated radio band is 123 MHz wide and centered at a frequency of 2130 MHz. The analog waveform consists of 1000 OFDM symbols, and is generated by an arbitrary waveform generator

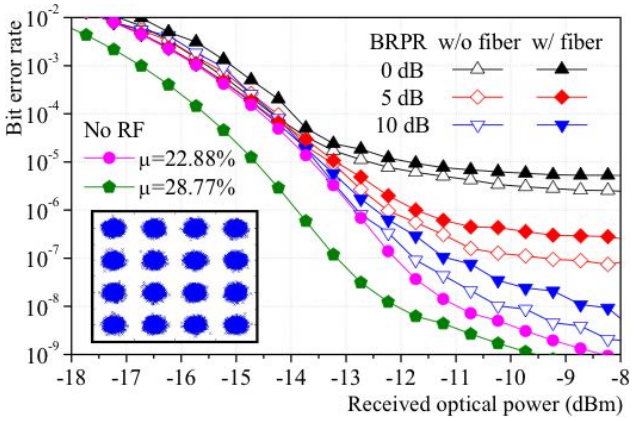

Fig. 10. Experimental results.

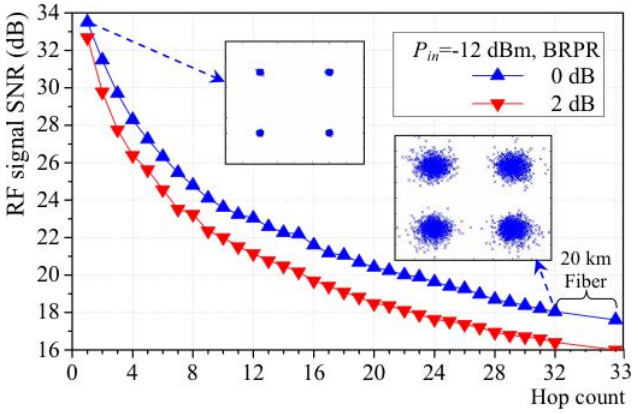

Fig. 11. Recirculating-loop experimental results of RF performance.

(AWG1). To generate the wireless signal, we follow WiMAX's format and use another AWG (AWG2) to produce three 20 MHz bandwidth RF signals at 2100 MHz, 2130 MHz, and 2160 MHz, respectively.

To evaluate downstream performance and fiber impairment, OFDM and RF signals are combined by a directional coupler to drive an intensity modulation optical transmitter that is of 5 dBm output power, 2.5 GHz bandwidth, and 1550 nm. Note that two electrical attenuators are applied to set the BRPR value. The spectrum density of the combined signal is shown in the right inset of Figure 9. For the direct link test, the combined signal reaches the PIN-based photoreceiver after traveling a 20 km single mode fiber and passing through an optical attenuator, which emulates the component loss and tests the receiver sensitivity. The received signal is split into two paths. For OFDM demodulation, a 50 GHz sampling rate real-time scope captures the signal for offline DSP processing, which is described in Section 3. On the other path, an 80 MHz bandwidth bandpass filter at 2130 MHz is implemented to extract the wireless signal for offline demodulation.

To assess the performance of the RF signal after it has cascaded through O-E-O conversions and also accumulated interference from the OFDM signal, an offline recirculating-loop experiment is executed. As shown in the lower part of Figure 9, a tap coupler, an optical photoreceiver, and a bandpass filter are used to extract RF signals. Using a 12.5 GHz sampling rate, a real-time scope then captures and stores a 20M section of the waveform in a file. After the waveform is stored, it is re-sampled to 12 GHz by a DSP program and fed to the AWG2 for the next hop transmission. For each hop, we load different OFDM signals to AWG1 so that the hops' interferences would not be correlated. In this way, we could emulate the accumulated interference imposed on the RF signal from ONU-1 to ONU-32.

B. Experimental Results

In Figure 10, we plot the BER curves of the OFDM signal under different BRPR values both before and after 20 km fiber transmissions. The notch filter order is set to $k = 400$. The back-to-back receiver sensitivity of OFDM for BER=10^{-4} is -14.6 dBm for u=22.88%. With these settings, when the RF signal is added to the link at BRPR=0 dB, only a 0.3 dB penalty is observed. After 20 km fiber transmissions, the receiver sensitivity is degraded by an additional 0.3 dB to -14 dBm. The OFDM constellation diagram (at BRPR=0 dB and receiver power=-10 dBm), is shown in the inset of Figure 10. The experimental results of the back-to-back SNR curves of the RF signal with respect to BRPR and optical receiver power are displayed and compared side-by-side with simulation results in Figure 7. We observe that experimental results are in agreement with the simulation results.

The results for the RF signal upstream based on the recirculating-loop experiment are shown in Figure 11. The optical received power is fixed at -12 dBm. As the node number increases, the SNR of the RF signal degrades due to the interference from the OFDM signal's side lobes. As expected from the analysis results in Section 4, if BRPR is equal to 2 dB, the SNR of the RF signal at the OLT can still remain above 16 dB after passing through 32 ONU's and a 20 km single mode fiber. We also show in the insets of Figure 11 the constellation diagrams of a QPSK-encoded wireless signal before and at the end of the recirculating loop, respectively.

We observe from the above results that the system performance is profoundly dependent on the receiver power, BRPR, and notch filter order. To protect the RF signal against accumulated interference from OFDM after 32 ONU's, the BRPR is required to be less than 2 dB and the upstream receiver power of each ONU must be greater than -12 dBm. Because the link loss between ONU's mainly comes from the two short feeder fibers, two circulators, and one coupler. Assuming a 1 dB insertion loss for feeder fiber and circulator, a 3 dB coupler is adopted in the ODD. The link loss between adjacent ONU's is 7 dB. Therefore, with over 5 dBm power for the optical transmitter, -12 dBm of receiver power in the upstream wavelength will provide a 17 dB power budget, which is sufficient to cover a 7 dB link loss. If we set the BRPR to $0 \sim 2$ dB, the order of OFDM receiver's notch filter needs to be greater than 400 to prevent a large power penalty from being imparted by the residual RF signal's interference. Experimental results show that when BRPR=0 dB, k=400, and 20 km fiber transmissions, the receiver sensitivity at 10^{-4} is -14 dBm. With a 6 dBm OLT transmitter power, there is a 20 dB optical power budget for ODD and fiber loss, which just meets the requirements of a 16-node system. The split ratio can be further improved by employing an avalanche

photo diode receiver (APD) receiver or a higher power optical transmitter [25].

VI. Conclusions

We have presented a novel OFDMA-PON architecture, ROFPON, which successfully integrates local broadband OFDM data and wireless RF signals from multiple remote antennas. In ROFPON, only two wavelengths, one for downstream and the other for upstream traffic, are required. Three 20 MHz WiMAX-format signals are overlaid on the 10 Gb/s broadband OFDMA signal. Furthermore, with the OFDM's high spectral efficiency, the combined signal occupies only 2.8 GHz. Experimental results show that after-coding direct-detection receiver sensitivity of OFDMA over a 20 km fiber is -14 dBm. The RF signal's robustness against OFDMA interference from ONU's is analyzed and demonstrated by running an offline recirculating loop experiment. Under a BRPR of 2 dB, the RF signal can be relayed in a 32 ONU's chain and recovered successfully.

References

[1] K. Grobe and J.-P Elbers, "PON in Adolescence: From TDMA to WDM-PON," *IEEE Commun. Mag.*, vol. 46, no. 1, Jan. 2008, pp. 26-34.

[2] M. Hajduczenia, H. J. A. Da Silva, and N. Borges, "Discovery Process for Emerging 10 Gb/s EPONs," *IEEE Commun. Mag.*, vol. 46, no. 11, Nov. 2008, pp. 82-90.

[3] K. Y. Cho, Y. Takushima, and Y. C. Chung, "10-Gb/s Operation of RSOA for WDM PON," *IEEE Photon. Tehcnol. Lett.*, vol. 20, no. 18, Sept. 2008, pp. 1533-1535.

[4] Y. M. Lin, "Demonstration and Design of High Spectrual Efficiency 4Gb/s OFDM System in Passive Optical Networks," *IEEE/OSA OFC*, 2007.

[5] T. N. Duong, N. Genay, M. Ouzzif, J. Le Masson, B. Charbonnier, P. Chanclou, and J. C. Simon, "Adaptive Loading Algorithm Implemented in AMOOFDM for NG-PON System Integrating Cost-Effective and Low-Bandwidth Optical Devices," *IEEE Photon. Technol. Lett.*, vol. 21, no. 12, June 2009, pp. 790-792.

[6] D. Qian, N. Cvijetic, J. Hu, and T. Wang, "A Novel OFDMA-PON Architecture with Source-Free ONUs for Next Generation Optical Access Networks," *IEEE Photon. Technol. Lett.*, vol. 21, no. 17, Sept. 2009, pp. 1265-1267.

[7] P. L. Tien, Y. M. Lin, and M. C. Yuang, "A Novel OFDMA-PON Architecture Toward Seamless Broadband and Wireless Integration," *IEEE/OSA OFC*, 2009.

[8] Y. M. Lin, P. L. Tien, M. C. Yuang, S. W. Lee, J. J. Chen, S. Y. Chen, Y. M. Huang, J. L. Shih, and C. H. Hsu, "A Novel Optical Access Network Architecture Supporting Seamless Integration of ROF and OFDMA Signals," *IEEE/OSA ECOC*, 2009.

[9] J. Armstrong, "OFDM for Optical Communications," *IEEE J. Lightwave Technol.*, vol. 27, no. 3, Feb. 2009, pp. 189-204.

[10] M. F. Huang, J. Yu, Z. Jia, and G. K. Chang, "Simultaneous Generation of Centralized Lightwaves and Double/Single Sideband Optical Millimeter-Wave Requiring Only Low-Frequency Local Oscillator Signals for Radio-Over-Fiber System," *IEEE J. Lightwave Technol.*, vol. 26, no.15, Aug. 2008, pp. 2653-2662.

[11] Q. Chang, Y Tian, J .Gao, T. Ye, Q. Li, and Y. Su, "Generation and Transmission of Optical Carrier Suppressed-Optical Differential (Quadrature) Phase-Shift Keying (OCS-OD(Q)PSK) Signals in Radio Over Fiber Systems," *IEEE J. Lightwave Technol.*, vol. 26, no. 15, Aug. 2008, pp. 2611-2618.

[12] D. Zibar, X. Yu, C. Peucheret, P. Jeppesen, and I. T. Monroy, "Digital Coherent Receiver for Phase-Modulated Radio-Over-Fiber Optical Link," *IEEE Photon. Technol. Lett.*, vol. 21, no. 3, Feb. 2009, pp. 155-157.

[13] M. Bakaul, A. Nirmalathas, C. Lim, D. Novak, and R. Waterhouse, "Hybrid Multiplexing of Multiband Optical Access Technologies Towards an Integrated DWDM Network," *IEEE Photon. Technol. Lett.*, vol. 18, no. 21, Nov. 2006, pp. 2311-2313.

[14] L. Chang, J. Wang, C. J. Chae, and A. Nirmalathas, "Combined Transmission of Baseband OFDM and PON Signals for Integrated Access Networks," *IEEE OECC/ACOFT*, 2008.

[15] P. T. Shih, C. T. Lin, W. J. Jiang, Y. H. Chen, J. J. Chen, and S. Chi, "Hybrid Access Network Integrated with Wireless Multilevel Vector and Wired Baseband Signals Using Frequency Doubling and No Optical Filtering," *IEEE Photon. Technol. Lett.*, vol. 21, no. 13, July 2009, pp. 857-859.

[16] L. Chen, J. G. Yu, S. Wen, J. Lu, Z. Dong, M. Huang, and G. K. Chang, "A Novel Scheme for Seamless Integration of ROF with Centralized Lightwave OFDM-WDM-PON System," *IEEE J. Lightwave Technol.*, vol. 27, no. 14, July 2009, pp. 2786-2791.

[17] H. Yamamoto, S. Morikura, K. Utsumi, and K. Fujito, "Increasing Acceptable Number of Signals in Subcarrier Multiple Access Optical Networks in the Presence of High Optical Beat Interference," *IEEE J. Lightwave Technol.*, vol. 17, no. 9, Sept. 1999, pp. 1525-1531.

[18] D. Qian, J. Hu, P. N. Ji, T. Wang, and M. Cvijetic, "10-Gb/s OFDMA-PON for Delivery of Heterogeneous Services," *IEEE/OSA OFC*, 2008.

[19] M. Crisp, S. Li, A. Watts, R. Penty, and I. H. White, "Uplink and Downlink Coverage Improvements of 802.11g Signals Using a Distributed Antenna Network," *IEEE J. Lightwave Technol.*, vol. 25, no. 11, Nov. 2007, pp. 3388-3395.

[20] T. Ohtsuki, "Multiple-Subcarrier Modulation in Optical Wireless Communicaitons," *IEEE Commun. Mag.*, vol. 41, no. 3, Mar. 2003, pp. 74-79.

[21] V. J. Urick, J. X. Qiu, and F. Bucholtz, "Wide-band QAM-over-fiber Using Phase Modulation and Interferometric Demodulation," *IEEE Photon. Technol. Lett.*, vol. 16, no. 10, Oct. 2004, pp. 2374-2376.

[22] T. Mizuochi, Y. Miyata, T. Kobayashi, K. Ouchi, K. Kuno, K. Shimizu, H. Tagami, H. Yoshida, H. Fujita, M. Akita, and K. Motoshima, "Forward Error Correction Based on Block Turbo Code with 3-bit Soft Decision for 10-Gb/s Optical Communication Systems," *IEEE J. Selected Topics Quantum Electron.*, vol. 10, no. 2, Mar.-Apr. 2004, pp. 376-386.

[23] F. Wang, A. Ghosh, C. SanKaran, P. Fleming, F. Hsieh, and S. Benes, "Mobile WiMAX Systems Performance and Evolution," *IEEE Commun. Mag.*, vol. 46, no. 10, Oct. 2008, pp. 41-49.

[24] J. G. Proakis and D. G. Manolakis, *Digital Signal Processing: Pinciples, Algorithms, and Applications*, Prentice-Hall 3rd edition, Chapter 8, USA, 1995.

[25] D. Qian, J. Hu, P. Nan Ji, and T. Wang, "10.8-Gb/s OFDMA-PON Transmission Performance Study," *IEEE/OSA OFC*, 2009.

[26] J. G. Proakis, *Digital Communications*, Chapter 5, 4th Edition, McGraw-Hill, 2001.

Yu-Min Lin received the B.S. degree in electrical engineering from National Tsing-Hua University, Taiwan, R.O.C., in 1996 and the Ph.D. degree in communication engineering from National Chiao-Tung University, Hsinchu, Taiwan, R.O.C., in 2003. He joined the Department of Optical Communications and Networks, Industrial Technology Research Institute (ITRI), Taiwan, R.O.C., in 2004. His research interests include broad-band optical networking and advanced modulation format for optical fiber communications.

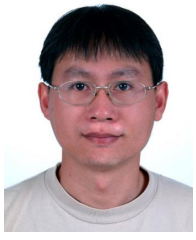

Po-Lung Tien received the B.S. degree in applied mathematics, the M.S. degree in computer and information science, and the Ph.D. degree in computer and information engineering, from the National Chiao Tung University, Taiwan, in 1992, 1995, and 2000, respectively. In 2005, he joined National Chiao Tung University, Taiwan, where he is currently an assistant professor of the department of communication engineering. His current research interests include optical networking, wireless networking, multimedia communications, performance modeling and analysis, and applications of soft computing.